Review of Scientific Instruments

Combining grating-coupled illumination and image recognition for stable and localized optical scanning tunneling microscopy

Cite as: Rev. Sci. Instrum. **94**, 023702 (2023); https://doi.org/10.1063/5.0123604
Submitted: 31 August 2022 • Accepted: 07 January 2023 • Published Online: 02 February 2023

Georg A. Traeger, Marlo H. Teichmann, Benjamin Schröder, et al.

Review of Scientific Instruments ARTICLE scitation.org/journal/rsi

Combining grating-coupled illumination and image recognition for stable and localized optical scanning tunneling microscopy

Cite as: Rev. Sci. Instrum. 94, 023702 (2023); doi: 10.1063/5.0123604
Submitted: 31 August 2022 • Accepted: 7 January 2023 •
Published Online: 2 February 2023

Georg A. Traeger,[1] Marlo H. Teichmann,[1] Benjamin Schröder,[1,2] and Martin Wenderoth[1,a)]

AFFILIATIONS

[1] IV. Physikalisches Institut, Georg-August-Universität Göttingen, Friedrich-Hund-Platz 1, 37077 Göttingen, Lower Saxony, Germany

[2] Max Planck Institute for Multidisciplinary Sciences, Am Faßberg 11, 37077 Göttingen, Lower Saxony, Germany

[a)] **Author to whom correspondence should be addressed:** martin.wenderoth@uni-goettingen.de

ABSTRACT

Combining scanning tunneling microscopy (STM) and optical excitation has been a major objective in STM for the last 30 years to study light–matter interactions on the atomic scale. The combination with modern pulsed laser systems even made it possible to achieve a temporal resolution down to the femtosecond regime. A promising approach toward a truly localized optical excitation is featured by nanofocusing via an optical antenna spatially separated from the tunnel junction. Until now, these experiments have been limited by thermal instabilities introduced by the laser. This paper presents a versatile solution to this problem by actively coupling the laser and STM, bypassing the vibration-isolation without compromising it. We utilize optical image recognition to monitor the position of the tunneling junction and compensate for any movement of the microscope relative to the laser setup with up to 10 Hz by adjusting the beamline. Our setup stabilizes the focus position with high precision (<1 μm) on long timescales (>1 h) and allows for high resolution STM under intense optical excitation with femtosecond pulses.

INTRODUCTION

Since the early days of scanning tunneling microscopy (STM), combining STM with optical excitation has been a major goal[1,2] not only because it promises a high temporal resolution beyond the bandwidth of high-gain current amplifiers but also because it can be employed to study light–matter interaction, such as photocatalysis.[3–9] Various approaches have been demonstrated covering a wide range of excitation conditions, including continuous wave,[3,10] multi-color,[11,12] or pulsed laser excitation,[4,13–15] as well as different excitation schemes, such as fiber coupled illumination,[3,15,16] macroscopic illumination,[10,17,18] or plasmonic near-fields, to increase the locality of the excitation.[3,19] Inspired by applications in scanning near-field optical microscopy (SNOM) and atomic force microscopy (AFM), a promising idea is the implementation of a remote excitation via optical antennas, e.g., gratings or nanocubes, that are spatially separated from the tunnel junction.[20–22] In all these efforts, the thermal effects induced by the laser excitation have been a severe issue.[13,15,23,24] Generally, the stability of the tunneling contact under optical excitation is one of the main reasons why STM combined with laser-based excitation is not widely used. The thermal effects can be divided into two categories. On the one hand, there are time-dependent variations of the laser power caused by, e.g., pulsed excitation, lock-in-detection, or laser power fluctuations, which result in variations of the STM tip length by thermal heating. These effects have been addressed in the past by introducing advanced pump–probe techniques such as shaken-pulse-pair excitation,[13–15] polarization modulation,[25] or pulse length modulation.[5] All techniques focus on keeping the average laser power and, therefore, the introduced thermal load as constant as possible. On the other hand, instabilities of the pointing, i.e., the position of the laser focus on the STM tip, that are caused due to a mechanical decoupling of the STM head and the laser system change the local thermal load and prevent a reliable

and reproducible operation. Moreover, the thermal effects have also been a showstopper for using more sophisticated approaches, such as grating couplers proposed by Müller *et al.*,[26] a technique that has already been applied for Tip Enhanced Raman Spectroscopy (TERS)[21,27,28] and promises truly localized excitations without a macroscopic background illumination of the sample by the laser focus.

This paper presents a versatile setup which utilizes image recognition and grating couplers for long-term STM measurements under a background-free femtosecond (fs) pulsed optical excitation of the tunnel junction. It is organized as follows: first, we introduce the basic concept of the grating-coupled gap excitation used in this paper and discuss its challenges with regard to thermal stability. Second, an experimental setup is introduced, which accounts for these problems by minimizing pointing instabilities, based on a method to track and eventually compensate for the relative movement of the laser focus and tunnel junction. Third, we demonstrate the performance by two examples: we image atomic scale defects during direct gap illumination of a tungsten tip and single atomic step-edges on an Ag(100) surface using purely ultrafast photocurrents[19] induced by a grating-coupled illumination of a gold tip during STM operation. Both can be done while maintaining a high stability of the STM operation.

GRATING-COUPLED GAP ILLUMINATION

Figures 1(a) and 1(b) illustrate two ways to realize an optical excitation in a tunnel junction. Conventionally, the laser is directly focused into the tunnel junction [see Fig. 1(a)]. Despite having a macroscopic focus of the order of 10 μm, it is possible to study local effects by utilizing the local field enhancement at the tip, which has been demonstrated by Kazuma *et al.*[3] Unfortunately, a vast majority of the light will just result in a delocalized excitation background. Consequently, most of the laser focus does not contribute to the excitation of the gap. This can be improved by utilizing grating couplers for gap illumination as illustrated in Fig. 1(b). Upon grating illumination, surface plasmon polaritons (SPPs) are launched and propagate to the tip apex, where they converge to a gap plasmon, resulting in a highly localized near-field on the order of a few nanometers.[29–32] This can be crucial for studies, e.g., surface photocatalysis, in which possible reaction pathways may include long living charge carriers in the substrate. Consequently, removing the macroscopic background illumination facilitates distinguishing the effects of the locally excited carriers from those excited by the macroscopic background due to the μm-scale laser focus.

All experiments presented in the following are performed with a home built low-temperature STM operating at 80 K in ultra-high vacuum (UHV). Our grating tips are made from gold wires (250 μm diameter, annealed for 16 h at 800 °C) to minimize propagation losses of the plasmon. The taper is prepared by electrochemical etching in a 37% hydrochloric acid solution (details can be found in Refs. 33 and 34). An efficient SPP excitation is provided by a resonant grating milled into the tip shaft by focused ion beam etching. To characterize the proposed stabilization mechanism, we use a single crystalline Ag(100) sample, which was prepared according to a standard recipe, consisting of repeated argon ion sputtering and annealing cycles under UHV conditions.[35] In order to position the focus (20 μm diameter) on the tip (apex-grating distance of 50 μm and grating periodicity of 1075 nm), we raster-scan the focus across the tip and sample (see the supplementary material for details). This allows us to measure the optically driven photocurrents as a function of focus position. The geometry as well as the result of such a measurement is shown in Fig. 1(c). Discriminating the optically induced signals from regular tunneling is done by retracting the tip by 5 Å from the tunnel contact (setpoint: 200 pA @ 2 V) before each current measurement.[19] The recorded map [right-hand side of Fig. 1(c)] shows three distinct features labeled as *G*, *A*, and *G*′. The signal indicated with *G* is the result of a gap excitation via the grating illumination, whereas the feature (*A*) originates from the direct apex illumination. Since the Ag sample is highly reflective, there appears an additional signal labeled G′ caused by a grating excitation by the reflected beam.

To further characterize the two excitation methods (apex vs. grating illumination), we analyzed the dependence of the photo-induced current on the tip–sample distance [retraction curves in

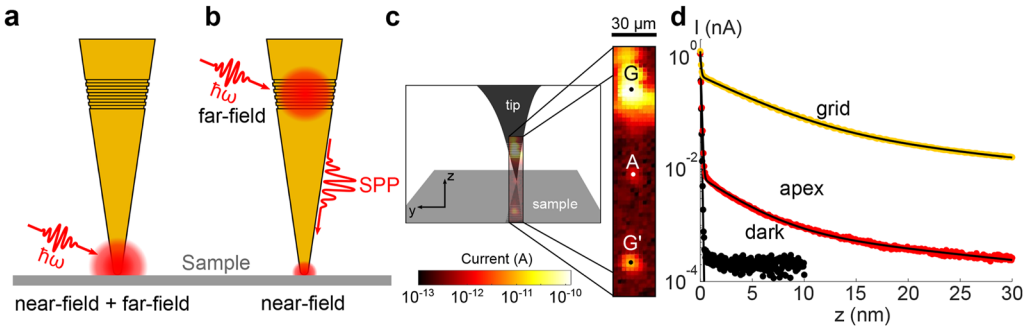

FIG. 1. Sketches of the applied excitation schemes: (a) conventional apex excitation, i.e., the far-field is directly focused into the tunneling gap, and (b) grating-based gap illumination. Here, a surface plasmon polariton (SPP) is launched by the grating coupler illumination and propagates to the junction resulting in a highly localized (near-field) excitation. (c) A typical focus raster scan across a tip–sample junction (setpoint: 200 pA @ 2 V; average laser power: 7 mW). A detailed description of the measurement can be found in the text. (d) The distance dependence of the current under grid (yellow) and apex (red) illumination (setpoint: 1 nA @ 4 V; average laser power: 7 mW), along with a reference curve without illumination (black, 1 nA @ 2 V). The solid lines are tri-exponential fits to the data.

Fig. 1(d)]. For both apex [Fig. 1(d), red line] and grating illumination [Fig. 1(d), yellow line], we find a steep decrease in the current for z < 1 nm, which resembles the exponential decay prominent in regular tunneling (black line). In addition, for distances >1 nm, both curves exhibit significant current contributions with a much lower decay length. These have been attributed to the charge transfer of non-equilibrium electrons at the junction.[19] Most importantly, it clarifies that the signal observed upon grating illumination in Fig. 1(c) originates from a gap excitation and is not an "ordinary" photocurrent emitted directly from the grating, as in that case, a distance-*independent* photocurrent would be expected. We highlight that the signal obtained using grating illumination is about two orders of magnitude larger compared to the gap illumination, despite the fact that both curves have been recorded using the same laser power. We attribute this to the fact that the μm-sized grating, compared to the nanometric apex, provides a much better focus overlap overcompensating for the propagation losses of the surface plasmon polariton, resulting in an overall better conversion efficiency. Similar observations have been made for free-standing tips.[26,36,37]

On the one hand, the higher efficiency of the grating illumination makes it possible to reduce the average laser power for a given excitation intensity at the apex. On the other hand, the better focus overlap leads to an increased absolute thermal load deposited in the tip for a given laser power and, therefore, to a higher tip expansion.[15] Which aspect dominates depends on multiple factors such as the tip diameter at the grating and the nonlinearity of the process under investigation. In general, both excitation methods are extremely sensitive to the spatial movements of the focus: a small drift of the focus position on the grating area in the order of a few micrometers will lead to thermal instabilities and can change the signal by more than an order of magnitude [see Fig. 1(c)]. While these movements are negligible for measurements performed on a short timescale (≈1 s), such as the retraction curves discussed above, they become a rapidly growing problem for measurements on the timescale of minutes and make it impossible to perform long-term measurements such as spatially resolved tunneling spectroscopy with acquisition times of several hours. To address this issue, we developed an active stabilization based on image recognition, which is described in the following.

STABILIZATION OF THE FOCUS

To realize STM with a laser excitation, one has to combine two opposing aspects: on the one hand, both systems must be mechanically and electronically decoupled for an efficient vibration isolation of the STM-head and noise free tunneling operation. On the other hand, the laser focus must be rigidly positioned onto the tip–sample system in order to avoid the thermal instabilities caused by a time-dependent laser heating. Hence, a versatile stabilization must be able to actively couple the two systems without any mechanical connections, which would compromise the vibration isolation. Furthermore, it is desirable to do this without adding any new components to the UHV system, to achieve maximum flexibility and easy handling.

In our case, the vibration isolation of the STM setup is achieved by two passive decoupling stages consisting of an air suspension and a set of metal springs. The air suspension is seated below the STM baseplate, and the springs decouple the microscope head from the STM baseplate. While this method properly isolates the STM-head mechanically, vibrations can still disturb the measurements by influencing the relative alignment of the tip and laser beam, which is located on a separate table next to the STM. In other words, it is necessary to couple three frames of reference (FoRs): the first one is the optical table with the laser (FoR1), the second one is the STM baseplate (FoR2), and finally, the third one is the STM head (FoR3) comprising the tip and sample. We achieved a coupling of these FoRs with an active stabilization consisting of two independent stages: first, a beam stabilization that couples FoR1 to FoR2 operating with up to 1 kHz and, second, an image stabilization that stabilizes FoR3 with respect to FoR2.

The first stage (beam stabilization) is based on two lateral effect position detectors[38] in combination with two piezo-controlled mirror mounts [PD1, PD2, PM1, and PM2 in Fig. 2(a)]. If set up with a minimum distance between the PD and their closest mirror as shown in Fig. 2(a), they act as virtual pinholes and allow for a well-defined beam alignment on the STM baseplate, thus compensating for beam tilting and parallel displacement.

Since the beam stabilization only couples FoR1 to FoR2, a second stage is needed to compensate for the relative movements of the tip (FoR3) with respect to the STM baseplate (FoR2). Inspired by the active image stabilization techniques in modern camera lenses, this is done by monitoring the tip with a CCD camera and moving the imaging lens, which projects the object on the camera chip or—in our case—creates an intermediate image of the tip in the image plane on the STM baseplate. This image plane (IP) is indicated by the purple line in Fig. 2(a). Any movement of the tip's position will result in a corresponding movement in the IP. To counteract this movement, it is necessary to track the tip's position and compensate for any deviation from the initial position by moving IL2 accordingly.

Determining the position of the tip is done using an image recognition routine. We observe the image plane through a magnification setup (20:1) using a CCD camera. The position of the tip can continuously be located by template matching as implemented in OpenCV.[39] More precisely, we determine the position maximum for the correlation function as

$$R(x,y) = \frac{\sum_{x',y'}\left(T'\left(x',y'\right) * I\left(x+x',y+y'\right)\right)}{\sqrt{\sum_{x',y'} T'(x',y')^2 * \sum_{x',y'} I(x+x',y+y')^2}},$$

where I is the current CCD image and T' is a template image [blue frame in Fig. 2(b)] of the tip, which is recorded before activating the stabilization. Being able to track and compensate for the individual movements of the tip relative to the STM baseplate, we have implemented a feedback loop, which is illustrated in Fig. 2(b). Whenever a deviation of the tip position is detected, IL2 is moved in the opposite direction to counteract this movement and, therefore, stabilizes the tip's image in the IP. Notably, this setup only compensates for displacements in the y–z plane [the STM operation is much less sensitive to displacements in the x direction due to the large Rayleigh length (≈400 μm) of the laser focus setup].

Finally, both independently operating stabilization stages are linked by a beam combiner (BC) and a scanning lens (SL). The BC

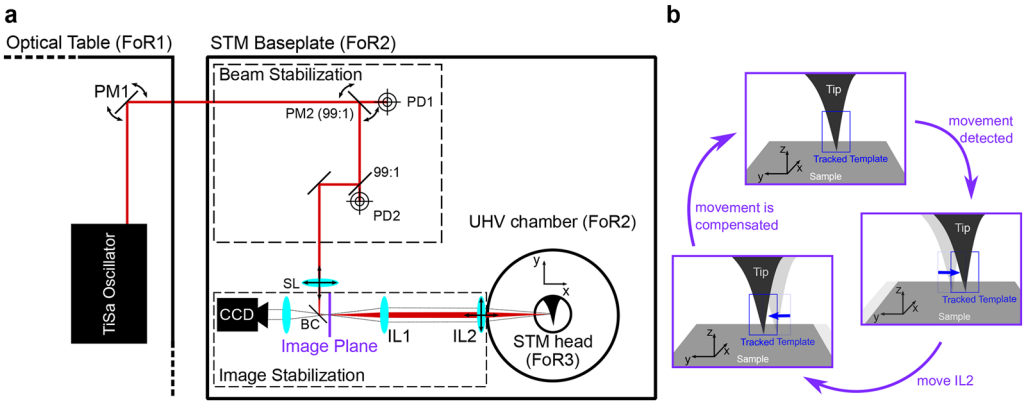

FIG. 2. (a) Schematic drawing of our setup (top view). It can be divided into three frames of reference (FoRs): a Ti:sapphire laser (λ_{Center} = 780 nm, τ = 15 fs, and 80 MHz repetition rate), placed on an optical table (FoR1), is guided onto the STM baseplate (FoR2) and coupled into the STM junction (FoR3) using our two-stage active coupling: (1) the beam stabilization consists of two position detectors (PD1 and PD2, Thorlabs PDP90A) and two piezo-controlled mirror mounts (PM1 and PM2, Polaris-K1S3P) and compensates for relative movements between STM baseplate (FoR2) and optical table (FoR1). (2) The image stabilization is based on the intermediate image plane (purple line) generated by the imaging lenses IL1 and IL2 (f = 200 mm) and is recorded by a CCD camera. The scanning lens (SL, f = 50 mm) focuses the laser beam into the intermediate image, which is consequently projected onto the tip (FoR3). (b) The image stabilization (side view), as observed through the beam combiner [BC in (a)] by the CCD camera. Unintended movements of the tip are detected by tracking a template of the tip (blue frame) and compensated for by moving the second imaging lens [IL2 in (a)].

is a dielectric mirror that reflects the laser light but is transparent for most visible light to allow the imaging of the IP by using the CCD camera. The scanning lens (SL) focuses the laser (stabilized by the beam stabilization) on the intermediate image of the tip (stabilized by the image stabilization). Since the optical pathway is reversible, this intermediate focus is simultaneously projected on the (real) tip in the STM-head. Consequently, the SL can be used to independently raster-scan the focus across the tip as demonstrated in Fig. 1(c) without compromising the overall stabilization. We note that this directly implies the requirement of a stable beam pointing at the position of the SL. In our case, this is ensured by the first stabilization stage described above, but—depending on the laser setup—it could also be achieved in other ways, e.g., by fiber coupling. A detailed description of the implementation and the specific components can be found in the supplementary material.

PERFORMANCE AND SPATIAL RESOLUTION

To quantify the long-term stability of the system, we use the raster-scan functionality shown in Fig. 1(c). Figure 3(a) shows a focus scan across a tungsten tip about 10 μm above an Ag(100) surface. Apart from the macroscopic shape of the tip, many localized features are visible. Figure 3(b) shows the consecutively acquired scans of the "hotspot" highlighted in Fig. 3(a), without active coupling. It becomes apparent that this hotspot, which had been in the center of the scan-area, drifts toward the right, indicating a movement of the tip with respect to the laser. From the data, we find a drift of roughly 10 μm/15 min in the y direction, which means that a perfectly adjusted setup would be misaligned after just a few minutes.

On the contrary, Fig. 3(c) shows that the active focus stabilization compensates for the drift as demonstrated by the perfectly centered signal feature even after 90 min. In practice, the stabilization has proven to completely eliminate the focus drift as a limiting factor for our measurement time. Eventually, this is limited by other aspects such as tip modifications or the coolant holding time. In addition, the setup allows for a fast (<15 min) realignment of the focus even after major interruptions of the measurements, such as coolant refilling. For a more quantitative description, we remove the background, i.e., any values that are below 10% of the maximum intensity, and determine the center of mass of the remaining peak. We achieve a focus stability better than 1 μm, which is limited by the resolution of the tracked image. The bandwidth of the setup is estimated to be of the order of 10 Hz considering the entire feedback loop (data transfer, processing, and IL2 stage movement).

To benchmark the performance during STM operation, we performed two experiments. First, we imaged the atomic scale defects using a tungsten tip at 150 μW apex illumination [see Fig. 4(a)]. This is a configuration that could be used for, e.g., the investigation of charge carriers in semiconductors.[16] Second, we analyzed a configuration that is useful for the investigation of photocatalysis, namely, the remote excitation of the tunnel gap via a grating coupler. Figure 4(b) shows a STM topography of a single atomic step-edge on an Ag(100) sample. The current consists mainly (>90%) of tunneling electrons energetically located at the Fermi level. In contrast, Fig. 4(c) shows a topography of the same area with a current composed of >98% of photo-driven high-energy electrons.[19] We quantify these distance-dependent contributions by fitting a bi-exponential function to the data [Fig. 4(d)]. The sum of tunneling (blue line) and the photo-driven current (yellow line) is shown as a black line resembling the data very closely. The fact that we are able to drive a nonlinear photocurrent[19] demonstrates that this test configuration facilitates a substantial gap excitation and could be applied to other sample systems. Noteworthily, all topographies shown in Fig. 4 have not been filtered except for a plane fit to remove the global slope of the sample.

As a measure for the stability of the system, we determined the root-mean-square (rms) of the apparent height variation (Δz) along

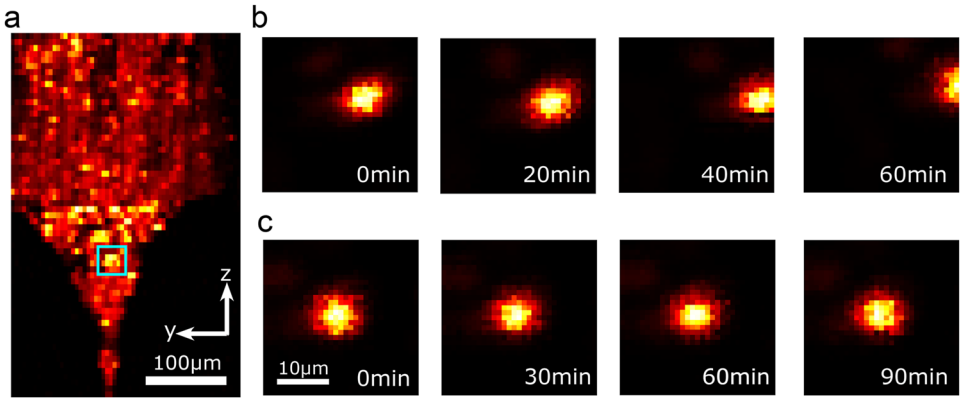

FIG. 3. (a) Map of the photocurrent recorded while raster scanning the laser focus across a tungsten tip using SL (logarithmic scale). The focus stability is examined by repeatedly raster scanning the focus across a photocurrent hotspot (cyan square). Raster-scanned photocurrent maps of the feature without and with active focus stabilization are shown in (b) and (c), respectively. The signal feature, observed with stabilization, remains centered for over 90 min.

the slow scan (vertical) axis on an actually flat terrace [see Fig. 4(e)]. This gives access to slow variations of the tip length, happening on a minute timescale. Both configurations show a z-stability better than 5 pm for the standard STM imaging. The section belonging to the photocurrent topography [yellow line in Fig. 4(e)] has a much higher variation of the order of 20 pm. This is not limited by thermal instabilities but by the small setpoint current (1.5 pA) in combination with the long decay length of the photo-driven current channel

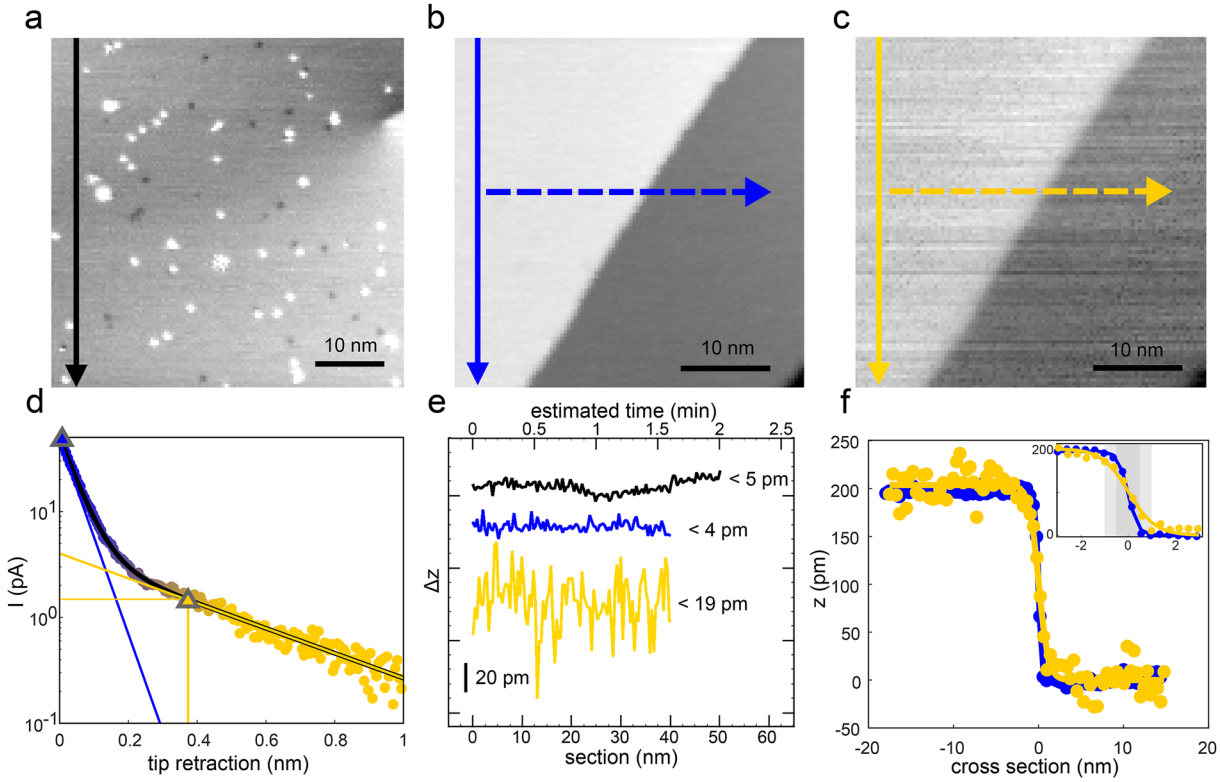

FIG. 4. (a) Constant-current STM topography (100 pA @ 1 V) of an Ag(100) surface, as imaged with a tungsten tip at 150 μW direct apex illumination, showing various atomic scale defects. (b) and (c) STM topographies, as imaged with a gold tip at 150 μW grating illumination. The different setpoints (50 pA @ 3 V and 1.5 pA @ 3 V, respectively) are chosen to address different tunneling channels, i.e., in the conventional tunneling regime (b) and the photo-driven regime (c). (d) Distance dependence of the tunnel current under grating illumination. The colored lines represent the two terms of the bi-exponential fit (black solid line) to the data, i.e., the conventional (blue) and laser induced (yellow) tunnel currents. The setpoints of (b) and (c) match the correspondingly colored triangles in (d). (e) Sections along the corresponding solid arrows in (a)–(c) with the respective root-mean-square (rms) denoted to the right of the section. The sections have been shifted in the z direction for clarity. (f) Cross sections along the dashed arrows in (b) and (c). The solid lines represent sigmoid fits to the step-edge. The broadening of the edge is illustrated by the inset, with gray boxes having a width of 1 nm (dark) and 2 nm (light).

(≈850 pm per order of magnitude compared to ≈110 pm per order of magnitude for regular tunneling). A variation of 20 pm corresponds to a current noise of about 80 fA, which is of the same order as the resolution of the analog-to-digital converter used in our STM setup. The low laser power (and, consequently, the low photocurrent setpoint) is a compromise to ensure comparability while accessing both the tunneling and the photocurrent regime at the same laser power. Considering the "high" temperature (~80 K) and "mobile" materials (gold tip/silver sample), this necessitates setpoints below 100 pA. A higher laser power would have required much higher tunneling currents (~nA) to reach a dominant tunnel contribution and inevitably caused tip modifications.

To estimate the lateral resolution of the photocurrent imaging, we analyze the cross sections of a step edge, which are shown in Fig. 4(f) and marked as dashed arrows with their respective colors in Figs. 4(b) and 4(c). By fitting sigmoid-type functions to the data, we extract step widths of <1 and <2 nm for the tunnel current and photocurrent data, respectively. It is worth mentioning that the illumination is the same for both images. The difference in the in-plane resolution is most likely caused by the different decay lengths of the two current channels used for imaging.

SUMMARY

We presented a versatile setup allowing for a reliable STM operation under a grating-coupled gap excitation by implementing an active coupling: Using a combination of a commercial beam stabilization and a home-built feedback based on image recognition, we are able to achieve a pointing stability better than 1 μm. This enables us to achieve a high stability during STM operation, i.e., height-variations of less than 5 pm under optical illumination. This is true for the direct apex illumination of tungsten tips as well as for the remote excitation via grating couplers on gold tips. The gap excitation via grating-launched surface plasmon polaritons provides substantial local photo-driven currents, sufficient to resolve single atomic steps on an Ag(100) crystal. Prospectively, the implemented stabilization allows for long-term STM measurements under an intense optical excitation, including pump–probe and spatially resolved spectroscopy of individual surface constituents such as molecules or defects.

SUPPLEMENTARY MATERIAL

See the supplementary material for a detailed description of the focus raster-scan procedure and the implementation of the image stabilization.

ACKNOWLEDGMENTS

This work was funded by the Deutsche Forschungsgemeinschaft (DFG, German Research Foundation) under Grant No. 217133147/SFB 1073 (Project No. C04).

AUTHOR DECLARATIONS

Conflict of Interest

The authors have no conflicts to disclose.

Author Contributions

Georg A. Traeger: Conceptualization (equal); Data curation (equal); Formal analysis (equal); Investigation (equal); Methodology (equal); Project administration (equal); Software (equal); Supervision (equal); Validation (equal); Visualization (equal); Writing – original draft (equal); Writing – review & editing (equal). **Marlo H. Teichmann**: Data curation (equal); Formal analysis (supporting); Investigation (equal); Methodology (equal); Software (equal); Validation (supporting); Visualization (supporting); Writing – review & editing (supporting). **Benjamin Schröder**: Data curation (supporting); Investigation (supporting); Methodology (equal); Software (supporting); Validation (supporting); Writing – review & editing (equal). **Martin Wenderoth**: Conceptualization (equal); Data curation (equal); Funding acquisition (equal); Methodology (equal); Project administration (equal); Resources (equal); Software (equal); Supervision (equal); Validation (equal); Writing – review & editing (equal).

DATA AVAILABILITY

The data that support the findings of this study are available from the corresponding author upon reasonable request.

REFERENCES

[1]R. J. Hamers and K. Markert, "Atomically resolved carrier recombination at Si(111)-(7 × 7) surfaces," Phys. Rev. Lett. **64**, 1051 (1990).
[2]R. J. Hamers and D. G. Cahill, "Ultrafast time resolution in scanned probe microscopies," Appl. Phys. Lett. **57**, 2031 (1990).
[3]E. Kazuma, J. Jung, H. Ueba, M. Trenary, and Y. Kim, "Real-space and real-time observation of a plasmon-induced chemical reaction of a single molecule," Science **360**, 521 (2018).
[4]T. L. Cocker, D. Peller, P. Yu, J. Repp, and R. Huber, "Tracking the ultrafast motion of a single molecule by femtosecond orbital imaging," Nature **539**, 263 (2016).
[5]M. Garg, A. Martin-Jimenez, Y. Luo, and K. Kern, "Ultrafast photon-induced tunneling microscopy," ACS Nano **15**, 018071 (2021).
[6]H. Böckmann, S. Liu, J. Mielke, S. Gawinkowski, J. Waluk, L. Grill, M. Wolf, and T. Kumagai, "Direct observation of photoinduced tautomerization in single molecules at a metal surface," Nano Lett. **16**, 1034 (2016).
[7]K. Morgenstern, N. Lorente, and K. H. Rieder, "Controlled manipulation of single atoms and small molecules using the scanning tunnelling microscope," Phys. Status Solidi B **250**, 1671 (2013).
[8]W. Ho, "Single-molecule chemistry," J. Chem. Phys. **117**, 11033 (2002).
[9]J. Lee, K. T. Crampton, N. Tallarida, and V. A. Apkarian, "Visualizing vibrational normal modes of a single molecule with atomically confined light," Nature **568**, 78 (2019).
[10]Y. Terada, S. Yoshida, A. Okubo, K. Kanazawa, M. Xu, O. Takeuchi, and H. Shigekawa, "Optical doping: Active control of metal-insulator transition in nanowire," Nano Lett. **8**, 3577 (2008).
[11]A. Dolocan, D. P. Acharya, P. Zahl, P. Sutter, and N. Camillone, "Two-color ultrafast photoexcited scanning tunneling microscopy," J. Phys. Chem. C **115**, 10033 (2011).
[12]X. Meng, W. Jin, H. Yang, J. I. Dadap, R. M. Osgood, A. Dolocan, P. Sutter, and N. Camillone, "Two-color field enhancement at an STM junction for spatiotemporally resolved photoemission," Opt. Lett. **42**, 2651 (2017).
[13].O. Takeuchi, H. Mogi, Z.-H. Wang, C. H. Yoon, A. Taninaka, S. Yoshida, and H. Shigekawa, "New delay-time modulation scheme for optical pump–probe scanning tunneling microscopy (OPP-STM) with minimized light-intensity modulation," Jpn. J. Appl. Phys. **58**, SIIA12 (2019).

[14]Y. Terada, M. Aoyama, H. Kondo, A. Taninaka, O. Takeuchi, and H. Shigekawa, "Ultrafast photoinduced carrier dynamics in GaNAs probed using femtosecond time-resolved scanning tunnelling microscopy," Nanotechnology **18**, 044028 (2007).
[15]P. Kloth, T. Thias, O. Bunjes, J. von der Haar, and M. Wenderoth, "A versatile implementation of pulsed optical excitation in scanning tunneling microscopy," Rev. Sci. Instrum. **87**, 123702 (2016).
[16]P. Kloth and M. Wenderoth, "From time-resolved atomic-scale imaging of individual donors to their cooperative dynamics," Sci. Adv. **3**, e1601552 (2017).
[17]P. Kloth, K. Kaiser, and M. Wenderoth, "Controlling the screening process of a nanoscaled space charge region by minority carriers," Nat. Commun. **7**, 10108 (2016).
[18]H. Shigekawa, O. Takeuchi, and M. Aoyama, "Development of femtosecond time-resolved scanning tunneling microscopy for nanoscale science and technology," Sci. Technol. Adv. Mater. **6**, 582 (2005).
[19]B. Schröder, O. Bunjes, L. Wimmer, K. Kaiser, G. A. Traeger, T. Kotzott, C. Ropers, and M. Wenderoth, "Controlling photocurrent channels in scanning tunneling microscopy," New J. Phys. **22**, 033047 (2020).
[20]M. Esmann, A. Chimeh, A. Korte, J.-H. Zhong, S. Stephan, J. Witt, G. Wittstock, N. Talebi, and C. Lienau, "Plasmonic nanofocusing spectral interferometry," Nanophotonics **9**, 491 (2020).
[21]X. Ma, Y. Zhu, N. Yu, S. Kim, Q. Liu, L. Apontti, D. Xu, R. Yan, and M. Liu, "Toward high-contrast atomic Force microscopy-tip-enhanced Raman spectroscopy imaging: Nanoantenna-mediated remote-excitation on sharp-tip silver nanowire probes," Nano Lett. **19**, 100 (2019).
[22]T. Jiang, V. Kravtsov, M. Tokman, A. Belyanin, and M. B. Raschke, "Ultrafast coherent nonlinear nanooptics and nanoimaging of graphene," Nat. Nanotechnol. **14**, 838 (2019).
[23]S. Grafström, P. Schuller, J. Kowalski, and R. Neumann, "Thermal expansion of scanning tunneling microscopy tips under laser illumination," J. Appl. Phys. **83**, 3453 (1998).
[24]O. Takeuchi, S. Yoshida, and H. Shigekawa, "Light-modulated scanning tunneling spectroscopy for nanoscale imaging of surface photovoltage," Appl. Phys. Lett. **84**, 3645 (2004).
[25]S. Yoshida, Y. Aizawa, Z.-h. Wang, R. Oshima, Y. Mera, E. Matsuyama, H. Oigawa, O. Takeuchi, and H. Shigekawa, "Probing ultrafast spin dynamics with optical pump-probe scanning tunnelling microscopy," Nat. Nanotechnol. **9**, 588 (2014).
[26]M. Müller, V. Kravtsov, A. Paarmann, M. B. Raschke, and R. Ernstorfer, "Nanofocused plasmon-driven sub-10 fs electron point source," ACS Photonics **3**, 611 (2016).
[27]S. Berweger, J. M. Atkin, R. L. Olmon, and M. B. Raschke, "Adiabatic tip-plasmon focusing for nano-Raman spectroscopy," J. Phys. Chem. Lett. **1**, 3427 (2010).
[28]K. Tomita, Y. Kojima, and F. Kannari, "Selective coherent anti-stokes Raman scattering microscopy employing dual-wavelength nanofocused ultrafast plasmon pulses," Nano Lett. **18**, 1366 (2018).
[29]C. Ropers, D. R. Solli, C. P. Schulz, C. Lienau, and T. Elsaesser, "Localized multiphoton emission of femtosecond electron pulses from metal nanotips," Phys. Rev. Lett. **98**, 043907 (2007).
[30]T. Umakoshi, M. Tanaka, Y. Saito, and P. Verma, "White nanolight source for optical nanoimaging," Sci. Adv. **6**, eaba4179 (2020).
[31]B. Schröder *et al.*, "Real-space imaging of nano-tip plasmons using electron energy-loss spectroscopy," Phys. Rev. B **92**, 085411 (2015).
[32]M. I. Stockman, "Nanofocusing of optical energy in tapered plasmonic waveguides," Phys. Rev. Lett. **93**, 137404 (2004).
[33]S. Schmidt, B. Piglosiewicz, D. Sadiq, J. Shirdel, J. S. Lee, P. Vasa, N. Park, D.-S. Kim, and C. Lienau, "Adiabatic nanofocusing on ultrasmooth single-crystalline gold tapers creates a 10-nm-sized light source with few-cycle time resolution," ACS Nano **6**, 6040 (2012).
[34]C. C. Neacsu, S. Berweger, and M. B. Raschke, "Tip-enhanced Raman imaging and nanospectroscopy: Sensitivity, symmetry, and selection rules," Nanobiotechnology **3**, 172 (2007).
[35]O. Bunjes, L. A. Paul, X. Dai, H. Jiang, T. Claus, A. Rittmeier, D. Schwarzer, F. Ding, I. Siewert, and M. Wenderoth, "Ordering a rhenium catalyst on Ag(001) through molecule-surface step interaction," Commun. Chem. **5**, 3 (2022).
[36]B. Schröder, M. Sivis, R. Bormann, S. Schäfer, and C. Ropers, "An ultrafast nanotip electron gun triggered by grating-coupled surface plasmons," Appl. Phys. Lett. **107**, 231105 (2015).
[37]J. Vogelsang, J. Robin, B. J. Nagy, P. Dombi, D. Rosenkranz, M. Schiek, P. Groß, and C. Lienau, "Ultrafast electron emission from a sharp metal nanotaper driven by adiabatic nanofocusing of surface plasmons," Nano Lett. **15**, 4685 (2015).
[38]W. Wang and I. J. Busch-Vishniac, "The linearity and sensitivity of lateral effect position sensitive devices—an improved geometry," IEEE Trans. Electron Devices **36**, 2475 (1989).
[39]G. Bradski, "The OpenCV Library," Dr. Dobb's J. Softw. Tools **25**(11), 120 (2000).